iJRASET
International Journal For Research in Applied Science and Engineering Technology

INTERNATIONAL JOURNAL FOR RESEARCH

IN APPLIED SCIENCE & ENGINEERING TECHNOLOGY

Volume: 7 **Issue:** V **Month of publication:** May 2019

DOI: https://doi.org/10.22214/ijraset.2019.5500

www.ijraset.com

Call: 08813907089 | E-mail ID: ijraset@gmail.com

International Journal for Research in Applied Science & Engineering Technology (IJRASET)
ISSN: 2321-9653; IC Value: 45.98; SJ Impact Factor: 7.177
Volume 7 Issue V, May 2019- Available at www.ijraset.com

Performane Improvement of Indoor and Outdoor Channel Models in Wireless Networks

Yuvraj Singh Ranawat[1], Suraj Kumhar[2]
[1,2]*Assistant Professor, Mewar University, Chittorgarh, India*

Abstract: ***A radio propagation model, also known as the radio frequency propagation model, is an empirical mathematical formulation for the characterization of radio wave propagation as a function of frequency, distance and other conditions .A single model is usually developed to predict the behavior of propagation for all similar links under similar constraints. Created with the goal of formalizing the way radio waves are propagated from one place to another, such models typically predict the path loss along a link or the effective coverage area of a transmitter.The channel model can vary with the antenna configuration in the transmitter and receiver (e.g., depending on single antenna system or multiple antenna system). Especially in the recent development of the multi-input and multi-output (MIMO) systems, acompletely different channel model is required to capture their spatio-temporal characteristics(e.g., the correlation between the different paths among the multiple transmit and receive antennas) [24]. This paper surveys different channel models used to characterise wireless indoor and outdoor environment. To develop and validate positioning algorithms under realistic conditions, an accurate knowledge of the propagation channel is significant. An outdoor-to-indoor channel model is proposed based on an extension of the geometry-based stochastic modeling approach to fulfill the requirements. The parameters of the outdoor-to-indoor channel model are extracted from two channel measurement campaigns. The proposed outdoor-to-indoor channel model is capable of accurately simulating the time variant channel. A comparison of the channel model with the channel measurement data is performed by comparing statistics.***
Keywords: SISO Channel models, MIMO, Doppler spectrum, Power delay profile (PDP), Doppler power spectrum (PSD).

I. INTRODUCTION

As high-speed data services for multimedia Internet access are brought to focus, huge date rates per user are anticipated for future 3G and 4G mobile radio systems. The most likely method of increasing capacity for wireless transmission is to exploit smart antennas. The algebraic framework is suitable for the description of SISO (single-input-single-output) radio transmission systems [8]. Channel models describe a communication channel and are essential in developing efficient wireless communication networks. The channel model can vary with the antenna configuration in the transmitter and receiver (e.g., depending on single antenna system or multiple antenna system).

Especially in the recent development of the multi-input and multi-output (MIMO) systems, a completely different channel model is required to capture their spatio-temporal characteristics (e.g., the correlation between the different paths among the multiple transmit and receive antennas). Fading properties of indoor wireless channels are quite different from those of mobile (vehicular) channels due to differences in the physical environment and the consequent differences in propagation mechanisms. In mobile wireless channels, 5–10 (and perhaps fewer) most significant paths are usually responsible for more than 80% of power delivered between the transmitter and receiver antennas. Rays along those paths undergo diffraction around vertical or horizontal edges of buildings, reflection off building surfaces, ground reflection, vegetation scattering, and so forth. If the dominant path to the receiver is shadowed by an obstacle, the total power may attenuate significantly, a phenomenon that earlier we called shadow fading.

II. INDOOR CHANNEL MODELS

The indoor channel corresponds to the small coverage areas inside the building, such as office and shopping mall. Since these environments are completely enclosed by a wall, the power azimuth spectrum (PAS) tends to be uniform (i.e., the scattered components will be received from all directions with the same power). Furthermore, the channel tends to be static due to extremely low mobility of the terminals inside the building. In the wireless digital communication systems, however, the degree of time variation in the signal strength is relative to the symbol duration. In other words, the channel condition can be considered static when the degree of time variation is relatively small with respect to the symbol duration. This particular situation is referred to as a quasi-static channel condition [12]. In fact, the indoor channels are usually modeled under the assumption that they have either static or quasi-static channel conditions.

ISSN: 2321-9653; IC Value: 45.98; SJ Impact Factor: 7.177
Volume 7 Issue V, May 2019- Available at www.ijraset.com

A. General Indoor Channel Models

In this subsection, we consider the two most popular indoor channel models: 2-ray model and exponential model. In the 2-ray model, there are two rays, one for a direct path with zero delay (i.e., $\tau_0 = 0$), and the other for a path which is a reflection with delay of $\tau_1 > 0$, each with the same power (see Figure 2.1 for its PDP) [5]. In this model, the maximum excess delay is $\tau_m = \tau_1$ and the mean excess delay τ is given as $\bar{\tau} = \tau_1/2$. It is obvious that the RMS delay is the same as the mean excess delay in this case (i.e., $\bar{\tau} = \sigma_\tau = \tau_1/2$. In other words, the delay of the second path is the only parameter that determines the characteristics of this particular model. However, it might not be accurate, simply because a magnitude of the second path is usually much less than that of the first path in practice. This model may be acceptable only when there is a significant loss in the first path.

In the exponential model, the average channel power decreases exponentially with the channel delay as follows:

$$P(\tau) = \frac{1}{\tau_d} e^{-\tau/\tau_d} \qquad (2.1)$$

where τ_d is the only parameter that determines the power delay profile (PDP). Figure 2.1 illustrates a typical PDP of the exponential model. This model is known to be more appropriate for an indoor channel environment. The mean excess delay and RMS delay spread turn out to be equal to each other, that is, $\bar{\tau} = \tau_d$ and $\bar{\tau} = \tau_\tau = \tau_d$, in the exponential model. Meanwhile, the maximum excess delay is given as

$$\tau_m = -\tau_d \ln A \qquad (2.2)$$

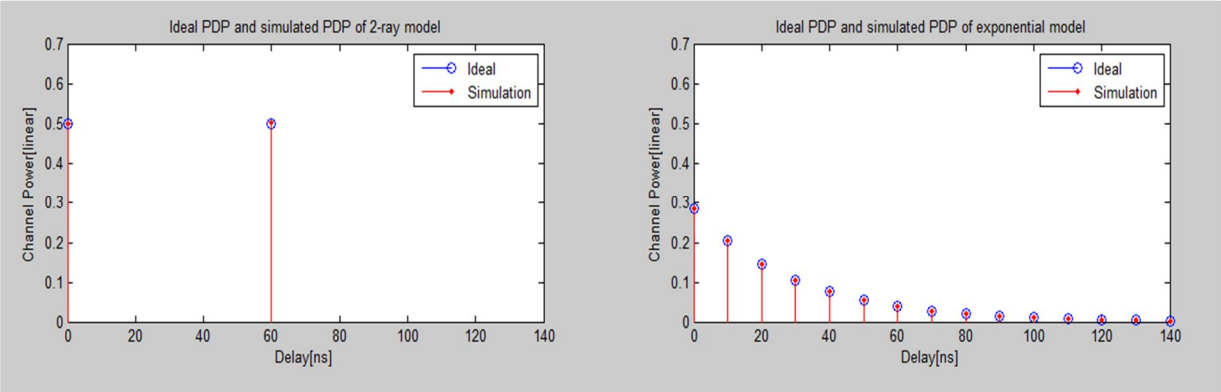

Figure 2.1 2-ray model vs. exponential model: an illustration.

where A is a ratio of non-negligible path power to the first path power, that is, $A = P(\tau_m)/P(0) = \exp(-\tau_m/\tau_d)$. Note that Equation (2.1) can be represented by the following discrete-time model with a sampling period of T_s

$$P(p) = \frac{1}{\sigma_\tau} e^{-pT_s/\sigma_\tau}, p = 0,1,.....,p_{max} \qquad (2.3)$$

where p is the discrete time index with p_{max} as the index of the last path, that is, $p_{max} = [\tau_m / T_s]$. A total power for the PDP in Equation (2.3) is given as

$$P_{total} = \sum_{p=0}^{p_{max}} P(p) = \frac{1}{\sigma_\tau} \cdot \frac{1 - e^{-(p_{max}+1)T_s/\sigma_\tau}}{1 - e^{-T_s/\sigma_\tau}} \qquad (2.4)$$

In order to normalize the total power in Equation (2.4) by one, Equation (2.3) has been modified as

$$P(p) = P(0) e^{-pT_s/\sigma_\tau}, p = 0,1,.....p_{max} \qquad (2.5)$$

where P(0) is the first path power.

B. IEEE 802.11 Channel Model

IEEE 802.11b Task Group has adopted the exponential model to represent a 2.4 GHz indoor channel [23]. Its PDP follows the exponential model as shown in Section 2. A channel impulse response can be represented by the output of finite impulse response (FIR) filter. Here, each channel tap is modeled by an independent complex Gaussian random variable with its average power that follows the exponential PDP [4], while taking the time index of each channel tap by the integer multiples of sampling periods. In other words, the maximum number of paths is determined by the RMS delay spread st and sampling period Ts as follows:

$$p_{\max} = [10.\sigma_\tau / T_s] \quad (2.6)$$

Assuming that the power of the pth channel tap has the mean of 0 and variance of $\sigma_p^2 / 2$, its impulse response is given as

$$h_p = Z_1 + j.Z_2, p = 0,....., p_{\max} \quad (2.7)$$

where Z1 and Z2 are statistically independent and identical Gaussian random variables, each with $N(0,\sigma_p^2 / 2)$.

As opposed to the exponential model in which the maximum excess delay is computed by a path of the least non-negligible power level, the maximum excess delay in IEEE802.11 channel model is fixed to 10 times the RMS delay spread. In this case, the power of each channel tap is given as

$$\sigma^2_p = \sigma_0^2 e^{-pT_s/\sigma_\tau} \quad (2.8)$$

where σ_0^2 is the power of the first tap, which is determined so as to make the average received power equal to one, yielding

$$\sigma_0^2 = \frac{1 - e^{-T_s/\sigma_\tau}}{1 - e^{-(p_{\max}+1)T_s/\sigma_\tau}} \quad (2.9)$$

In the IEEE 802.11 channel model, a sampling period Ts must be at least as small as 1/4. Figure 2.2 shows the average channel power and channel frequency response for the IEEE 802.11 channel model. Since the RMS delay spread is relatively small in this example, the power variation in the frequency domain is within at most 15dB, which implies that frequency selectivity is not that significant [22].

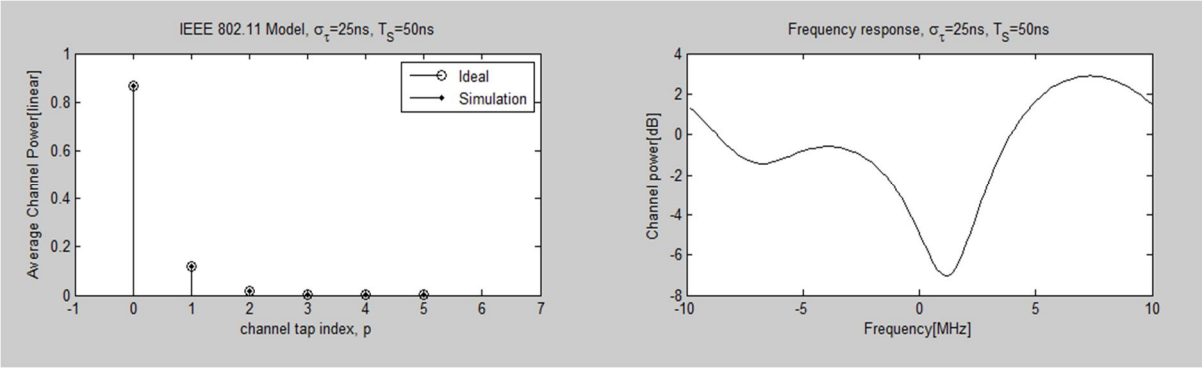

(a) Average channel power (b) Channel frequency response

Figure 2.2 IEEE 802.11 channel model.

C. Saleh-Valenzuela (S-V) Channel Model

It has been verified by intense measurements of the indoor channel that arrivals of the multipathdelayed components can bemodeled as a Poisson process. More specifically, Saleh and Valenzuela have proposed a new channel model (referred to as S-V channel model) after finding from the indoor channel measurements that there are multiple clusters, eachwithmultiple rays, in the delay profile [24].

The S-V channel model with multiple clusters, each of which is associated with a set of rays. The arrival times of each cluster as well as rays in each cluster follow an individual Poisson process. Therefore, the delay of each path is not spaced in the multiple of sampling periods, but spaced in a rather arbitrary manner [24]. More specifically, the arrival time of the first ray in the mth cluster, denoted by T_m, is modeled by a Poisson process with an average arrival rate of Λ while the arrival times of rays in each cluster is modeled by a Poisson process with an average arrival rate of λ. Then, it can be shown that a distribution of inter-cluster arrival times and a distribution of inter-ray arrival times are given by the following exponential distributions, respectively [25]:

$$f_{T_m}\left(T_m \middle| T_{m-1}\middle|\right) = \Lambda \exp[-\Lambda(T_m - T_{m-1})], \mathrm{m} = 1, 2, ... \quad (2.10)$$

and

$$f_{\tau_{r,m}}\left(\tau_{r,m} \middle| \tau_{(r-1),m}\middle|\right) = \lambda \exp[-\lambda(\tau_{r,m} - \tau_{(r-1),m})], \mathrm{r} = 1, 2, ... \quad (2.11)$$

where $\tau_{r,m}$ denotes the arrival time of the rth ray in the mth cluster. In Equation (2.10) and Equation (2.11), the arrival time of the first ray in the mth cluster, $\tau_{0,m}$, is defined as the arrival time of themth cluster, T_m (i.e., $\tau_{0,m} = T_m$). Let $\beta_{r,m}$ and $\theta_{r,m}$ denote amplitude and phase of the rth ray in the mth cluster, respectively. Then, a channel impulse response is given as

$$h(t) = \sum_{m=0}^{\infty}\sum_{r=0}^{\infty}\beta_{r,m}e^{j\theta_{r,m}}\delta(t - T_m - \tau_{r,m}) \quad (2.12)$$

where $\theta_{r,m}$ is a random variable that is uniformly distributed over $(0, 2\Pi)$ and $\beta_{r,m}$ is an independent random variable with the following Rayleigh distribution:

$$f_{\beta_{r,m}}(\beta_{r,m}) = \left(2\beta_{r,m} / \overline{\beta^2}_{r,m}\right)e^{-\beta^2_{r,m}/\overline{\beta^2}_{r,m}} \quad (2.13)$$

In Equation (2.13), $\beta_{r,m}$ is the average power of the rth ray in the mth cluster, which is given as

$$\overline{\beta^2}_{r,m} = \overline{\beta^2}_{0,0}e^{-T_m/\Gamma}e^{-\tau_{r,m}/\gamma} \quad (2.14)$$

where Γ and γ denote time constants for exponential power attenuation in the cluster and ray, respectively, while $\beta^2_{0,0}$ denotes the average power of the first ray in the first cluster [21]. the S-V channelmodel is a double exponential delay model in which average cluster power decays exponentially by following a term $e^{-T_m/\Gamma}$ in Equation (2.14)while average ray power in each cluster also decays exponentially by following a term $e^{-\tau_{r,m}/\gamma}$ in Equation (2.14). Once the average power of the first ray in the first cluster, $\beta^2_{0,0}$, is given, the average power of the rest of rays can be determined by Equation (2.14), which subsequently allows for determining the Rayleigh channel coefficients by Equation (2.13). In case that a path loss is not taken into account, without loss of generality, the average power of the first ray in the first cluster is set to one. Even if there are an infinite number of clusters and rays in the channel impulse response of Equation (2.12), there exist only a finite number of the non-negligible numbers of clusters and rays in practice. Therefore, we limit the number of clusters and rays to M and R, respectively. Meanwhile, a log-normal random variable X, that is, $20\log_{10}(X) \sim N(0, \sigma^2_x)$, can be introduced to Equation (2.12), so as to reflect the effect of long-term fading as

$$h(t) = X\sum_{m=0}^{M}\sum_{r=0}^{R}\beta_{r,m}e^{j\theta_{r,m}}\delta(t - T_m - \tau_{r,m}) \quad (2.15)$$

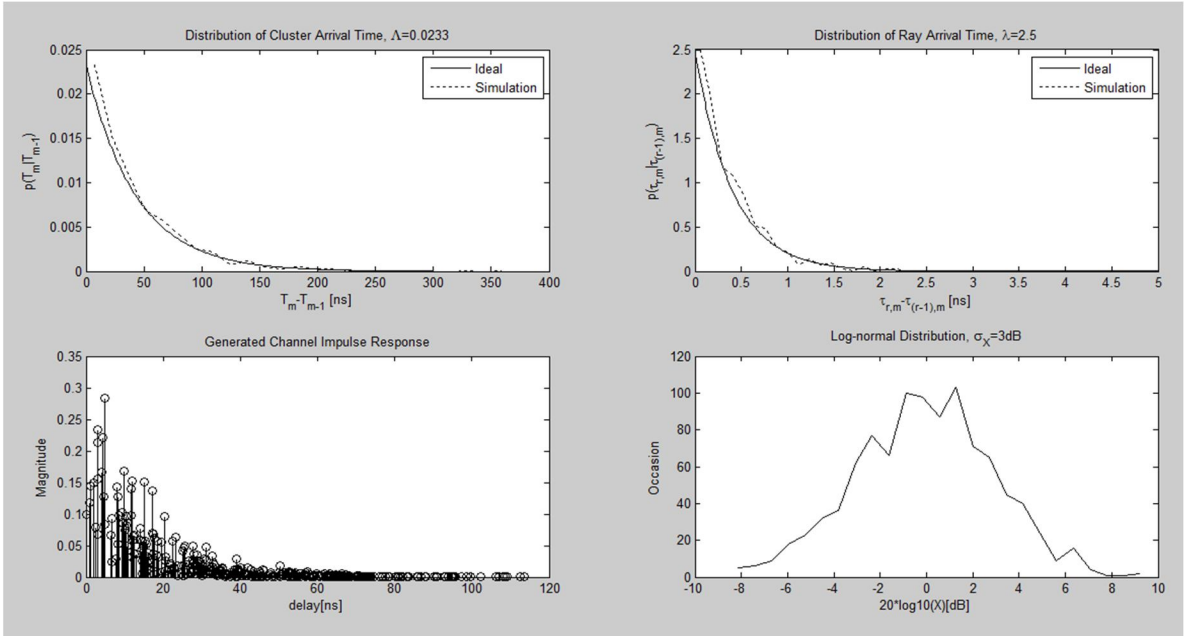

Figure 2.3 Saleh-Valenzuela channel model.

ISSN: 2321-9653; IC Value: 45.98; SJ Impact Factor: 7.177
Volume 7 Issue V, May 2019- Available at www.ijraset.com

Figures 2.3 show the distributions of cluster arrival times and ray arrival times, respectively, including the simulation results to be comparedwith the analytical ones where the mth cluster arrival time T_m and the rth ray arrival time $\tau_{r,m}$ in the mth cluster are generated in such a way that each of them has an exponential distribution of Equation (2.10) and Equation (2.11), respectively. Figure 2.3 shows the channel impulse response of theS-V channel. Figure 2.3, showing the channel power distribution, is obtained by simulating 1,000 channels, from which it is clear that the channel power follows a log-normal distribution [20].

D. UWB Channel Model

According to measurements of broadband indoor channel, it has been found that amplitudes of multipath fading follow the log-normal or Nakagami distribution rather than the Rayleigh distribution, even if they also show the same phenomenon of clustering as in the Saleh- Valenzuela (S-V) channel model. Based on these results, SG3a UWB multipath model has been proposed by modifying the S-V model in such a way that the multi-cluster signals are subject to independent log-normal fading while the multi-path signals in each cluster are also subject to independent log-normal fading [25].

The ith sample function of a discrete-time impulse response in the UWB multi-path channel model is given as

$$h_i(t) = X_i \sum_{m=0}^{M} \sum_{r=0}^{R} a^{(i)}_{r,m} \delta\left(t - T^{(i)}_m - \tau^{(i)}_{r,m}\right) \qquad (2.16)$$

where $X_i, a^{(i)}_{r,m}, T^{(i)}_{r,m}$ and $\tau^{(i)}_{r,m}$ are defined as the same as in Equation (2.15), nowwith the index i to represent the ith generated sample function of the channel. For simplicity of exposition, the index i in Equation (2.16) will be eliminated in the following discussion. As in the S-V channel model, the arrival time distributions of clusters and rays are given by two different Poisson processes of Equation (2.10) and Equation (2.11), respectively. The UWB channel model is different from the S-V channel model in that clusters and rays are subject to independent log-normal fading rather than Rayleigh fading. More specifically, a channel coefficient is given as

$$\alpha_{r,m} = p_{r,m} \xi_m \beta_{r,m} \qquad (2.17)$$

where ξ_m represents log-normal fading of the mth cluster with the variance of σ^2_1 while $\beta_{r,m}$ represents log-normal fading of the rth ray with the variance of σ^2_2 in the mth cluster. Note that independent fading is assumed for clusters and rays. In Equation (2.17), $p_{r,m}$ is a binary discrete random variable to represent an arbitrary inversion of the pulse subject to reflection, that is, taking a value of +1 or -1 equally likely. As compared to the channel coefficients of the S-V channel model in Equation (2.12) which has a uniformlydistributed phase over $[0, 2\Pi)$, those of UWB channel model have the phase of either $-\Pi$ or Π , making the channel coefficient always real [14]. Furthermore, we note that amplitude of each ray is given by a product of the independent log-normal random variables, ξ_m and $\beta_{r,m}$. Since a product of the independent log-normal random variables is also a log-normal random variable, a distribution of the channel coefficient $|\xi_m \beta_{r,m}| = 10^{(\mu_{r,m} + z_1 + z_2)/20}$ also follows a log-normal distribution, that is, $20\log_{10}(\xi_m \beta_{r,m}) \sim N\left(\mu_{r,m}, \sigma^2_1 + \sigma^2_2\right)$, with its average power given as

$$E\left[\left|\xi_m \beta_{r,m}\right|^2\right] = \Omega_0 e^{-T_m/\Gamma} e^{-\tau_{r,m}/\gamma} \qquad (2.18)$$

where Ω_0 represents the average power of the first ray in the first cluster.Meanwhile, mean of the channel amplitude for the rth ray in the mth cluster can be found as

$$\mu_{r,m} = \frac{10\ln(\Omega_0) - 10T_m/\Gamma - 10\tau_{r,m}/\gamma}{\ln(10)} - \frac{\left(\sigma^2_1 + \sigma^2_2\right)\ln(10)}{20} \qquad (2.19)$$

Besides the same set of channel parameters as in the S-V channel model, including the cluster arrival rate Λ, ray arrival rate λ, cluster attenuation constant Γ, ray attenuation constant γ, standard deviation σ_x of the overall multipath shadowing with a log-normal distribution, additional channel parameters such as the standard deviations of log-normal shadowing for the clusters and rays, denoted as σ_1 and σ_2, respectively, are required for the UWB channel model. Note that a complete model of the multipath

channel h(t) in Equation (2.16) is given as a real number. Some proper modifications such as downconversion and filtering are required for implementing the UWB channel in simulation studies, since its bandwidth cannot be limited due to arbitrary arrival times. All the channel characteristics for UWB channel model, including mean excess delay, RMS delay spread, the number of significant paths within 10dB of peak power (denoted as NP_{10dB}), and PDP, must be determined so as to be consistent with the measurements in practice.

Target channel characteristics	CM1	CM2	CM3	CM4
Mean excess delay (nsec) $(\bar{\tau})$	5.05	10.38	14.18	
RMS delay (nsec) (σ_τ)	5.28	8.03	14.28	25
NP_{10dB}			35	
NP(85%)	24	36.1	61.54	
Model parameters				
Λ (1/nsec)	0.0233	0.4	0.0667	0.0667
λ (1/nsec)	2.5	0.5	2.1	2.1
Γ	7.1	5.5	14.00	24.00
γ	4.3	6.7	7.9	12
σ_1 (dB)	3.3941	3.3941	3.3941	3.3941
σ_2 (dB)	3.3941	3.3941	3.3941	3.3941
σ_x (dB)	3	3	3	3
Model parameters				
Mean excess delay (nsec) $(\bar{\tau})$	5.0	9.9	15.9	30.1
RMS delay (nsec) (σ_τ)	5	8	15	25
NP_{10dB}	12.5	15.3	24.9	41.2
NP(85%)	20.8	33.9	64.7	123.3
Channel energy mean (dB)	-0.4	-0.5	0.0	0.3
Channel energy std (dB)	2.9	3.1	3.1	2.7

Table 2.1 UWB channel parameters and model characteristics [25].

Table 2.1 summarizes the SG3a model parameters and characteristics that represent thetarget UWB channel for four different types of channel models, denoted as CM1, CM2,CM3, and CM4. Each of these channel models varies depending on distance and whether LOS exists or not. Here, NP(85%) represents the number of paths that contain 85% of the total energy. CM1 and CM2 are based on measurements for LOS and Non-LOS environments over the distance of 0–4m, respectively. CM3 is based on measurement for a Non-LOS environment over the distance of 4–10m. CM4 does not deal with any realistic channel measurement, but it has been set up with the intentionally long RMS delay spread so as to model the worst-case Non-LOS environment [26]. CM1 shows the best channel characteristics with the short RMS delay spread of 5.28ns since it deals with a short distance under an LOS environment. Due to the Non-LOS environment, CM2 shows the longer RMS delay spread of 8.03ns, even if it has the short range of distance as in the CM1. Meanwhile, CM3 represents the worse channel with the RMS delay spread of 14.28; it has a longer distance under a Non-LOS environment.

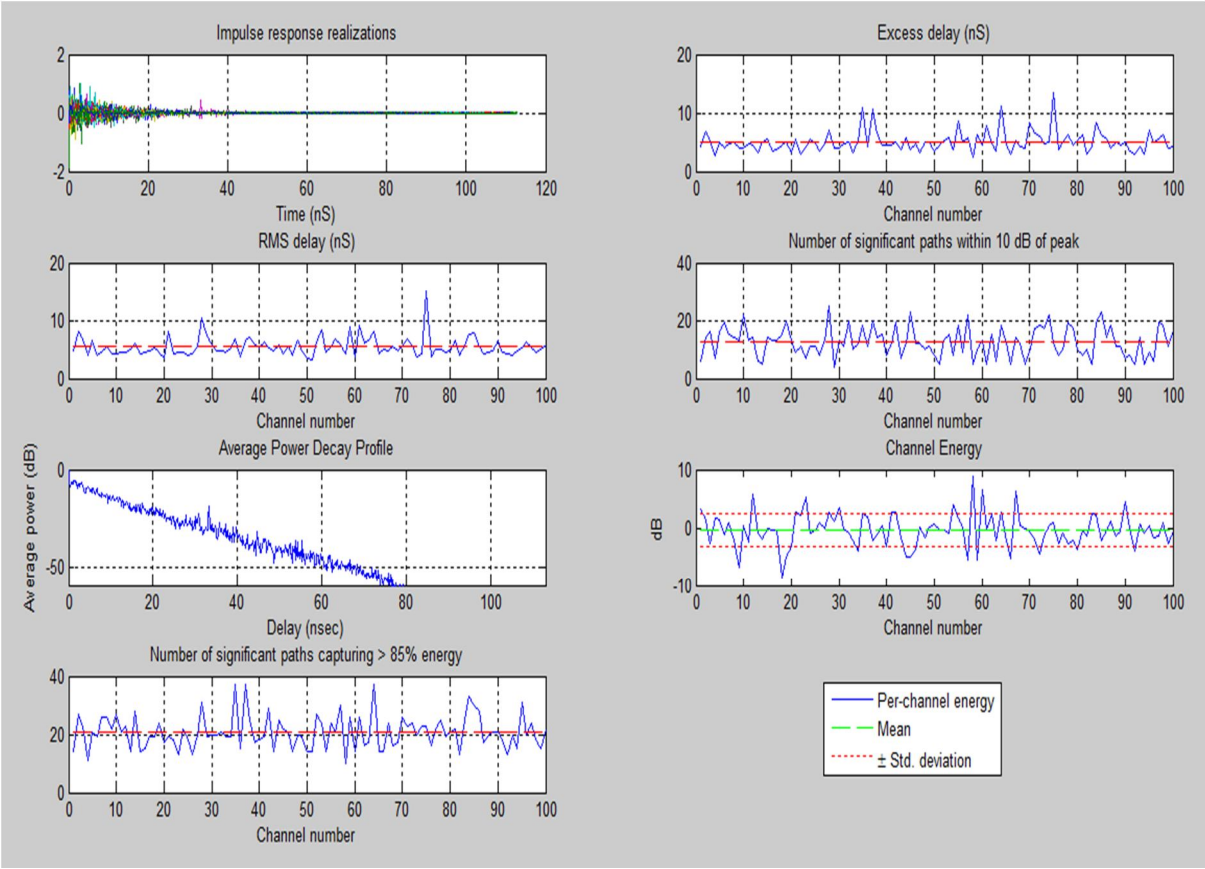

Figure 2.4 Generation of UWB channel: example (CM1).

Figure 2.4 shows UWB channel model are used to set the UWB channel parameters as listed in Table 2.1, to convert the continuous-time UWB channel into the corresponding discrete-time one, and to generate a UWB channel model, respectively. It shows the UWB channel characteristics by simulating 100 CM1 channels. Here, the sampling period has been set to 167 ps. In the current measurement, the RMS delay spread turns out to be around 5 ns, which nearly coincides with the target value of CM1 channel in Table 2.1. The same observation is made for the mean excess delay [24].

III. OUTDOOR CHANNEL MODELS

As opposed to the static or quasi-static nature of the indoor channel, outdoor channels are typically characterized by time variation of the channel gain, which is subject to the mobile speed of terminals. Depending on the mobile speed, time variation of channel gain is governed by Doppler spectrum, which determines the time-domain correlation in the channel gain. In this subsection, we discuss how to model the time-correlated channel variation as the mobile terminal moves. Furthermore, we present some practical methods of implementing the outdoor channel models for both frequency-flat and frequency-selective channels.

A. FWGN Model

The outdoor channel will be mostly characterized by Doppler spectrum that governs the time variation in the channel gain. Various types of Doppler spectrum can be realized by a filtered white Gaussian noise (FWGN) model. The FWGN model is one of the most popular outdoor channel models. The Clarke/Gans model is a baseline FWGN model that can be modified into various other types, depending on how a Doppler filter is implemented in the time domain or frequency domain.We first discuss the Clarke/Gans model and then, its frequency-domain and time-domain variants.

1) *Clarke/Gans Model:* The Clarke/Gans model has been devised under the assumption that scattering components around a mobile station are uniformly distributed with an equal power for each component [26]. Figure 3.1 shows a block diagram for the Clarke/Gans model, in which there are two branches, one for a real part and the other for an imaginary part. In each branch, a complex Gaussian noise is first generated in the frequency domain and then, filtered by a Doppler filter such that a frequency

component is subject to Doppler shift. Finally, the Doppler-shifted Gaussian noise is transformed into the time-domain signal via an IFFT block. Since output of the IFFT block must be a real signal, its input must be always conjugate symmetric. Constructing a complex channel gain by adding a real part to an imaginary part of the output, a channel with the Rayleigh distributed-magnitude is generated.

Figure 3.2 shows the time-domain characteristics of the frequency-non-selective fading channel with a Doppler frequency of $f_m = 100Hz$ and a sampling period of $T_s = 50\mu s$. From these results, it is observed that the channel gain is time-varying with the Rayleigh-distributed amplitude and uniformly-distributed phase. Variation of the channel amplitude becomes more significant as the Doppler frequency increases, demonstrating the fast fading characteristics

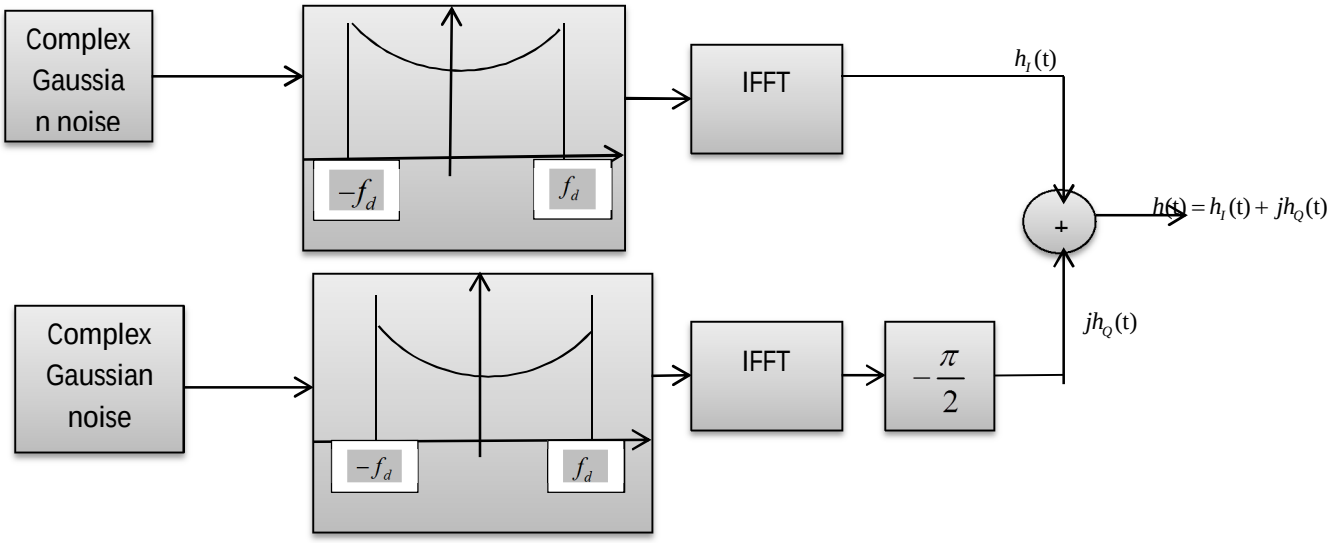

Figure 3.1 Block diagram for Clarke/Gans model.

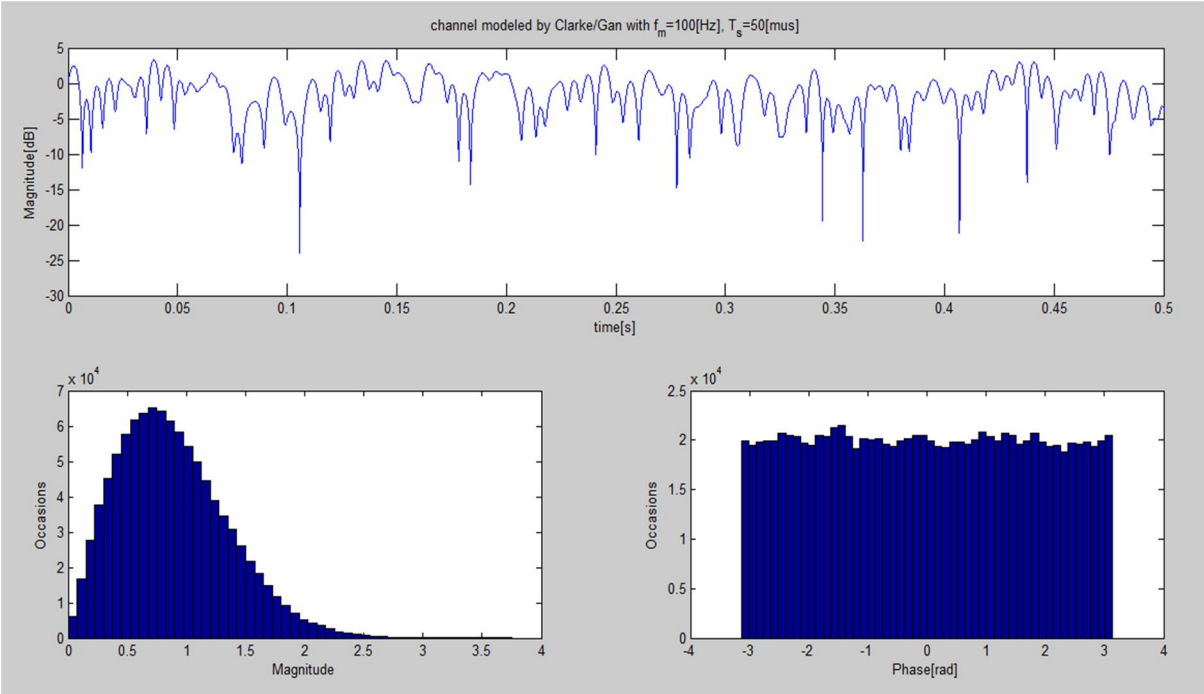

Figure 3.2 Generation of a time-varying channel with Clarke/Gans model. (a) Time-domain channel characteristics (b) Distribution of magnitude (c) Distribution of phase

2) Modified Frequency-Domain FWGN Model: Since the Clarke/Gans model employs two IFFT blocks, it has disadvantages of computational complexity. Among many other variants of the Clarke/Gans model, we here describe one used in I-METRA model.

Figure 3.3 describes a process of generating the Doppler spectrum. Let f_m denote the Doppler frequency. Since the spectrum repeats with respect to Nyquist frequency, $2f_m$, for normal sampling, it must be folded for an IFFT function to deal with the positive frequency components only as shown in Figure 3.3(a). When oversampled by a factor of NOS, the bandwidth of Doppler spectrum becomes $B_D = 2N_{os} f_m$ as shown in Figure 3.3(b). Its inverse $\Delta t = 1/B_D$ is the sample spacing in the time domain, which corresponds to the coherence time of the fading channel. Dividing the Doppler bandwidth into N_{Fading} subbands, each subband of the length $\Delta f_m = B_D / N_{Fading}$ leads to the overall length of the fading channel, given by $T_{Fading} = 1/\Delta f_m = N_{Fading} / B_D$. Meanwhile, Figure 3.3(c) shows a discrete-frequency Doppler spectrum and its equivalent discretetime fading channel. For the IFFT size of N_{Fading}, the frequency spacing of Doppler spectrum is

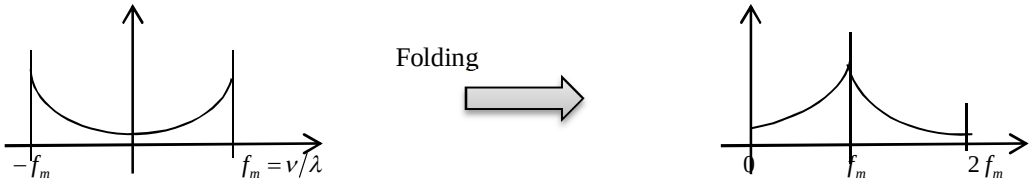

(a) Normal sampling

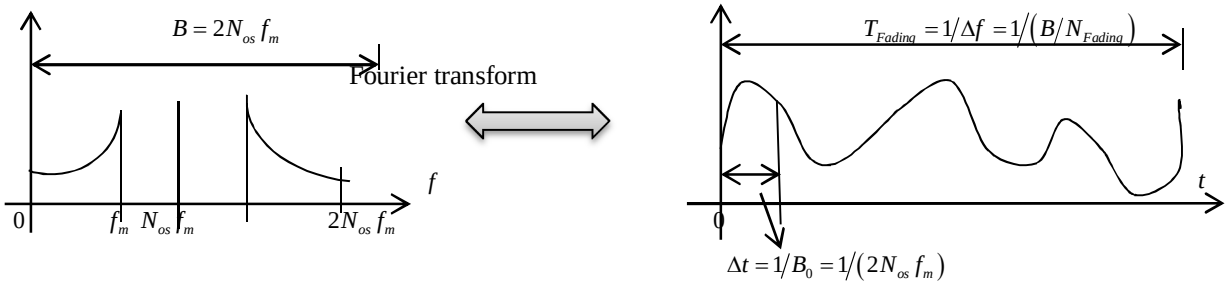

(b) Oversampling

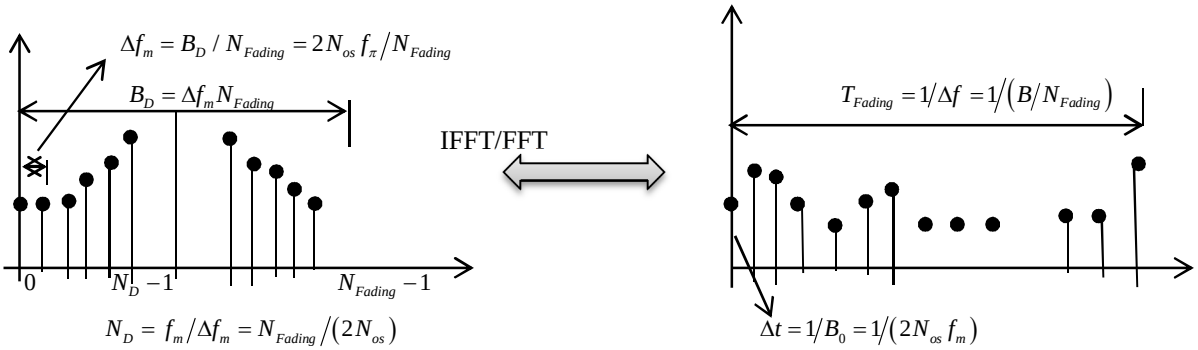

(c) Discrete-time oversampling

Figure 3.3 Generation of Doppler spectrum.

given by $\Delta f_m = 2N_{os} f_m / N_{Fading}$. The number of discrete-time frequency samples in the overall Doppler spectrum is given by $N_D = f_m/\Delta f_m = N_{Fading} / (2\,N_{os})$. This particular method allows for generating the fading signal with a given duration of T_{Fading} without taking the maximum Doppler frequency into account. Furthermore, it is advantageous for simulation since the time-domain signal can be obtained by interpolation with the maximum Doppler frequency f_m.

ISSN: 2321-9653; IC Value: 45.98; SJ Impact Factor: 7.177
Volume 7 Issue V, May 2019- Available at www.ijraset.com

Here, a magnitude of channel response can be computed from the Doppler spectrum with an arbitrary phase. A channel response of each path in the time domain is given as

$$h[n] = \sum_{k=-N_{Fading}/2}^{N_{Fading}/2-1} \sqrt{S[k]}\, e^{j\theta_k} e^{j2\Pi nk/N_{Fading}} \qquad (3.1)$$

where $S(k)$ is the Doppler spectrum at a discrete frequency $k = f/\Delta f_m, n = t/\Delta t$ is the discrete time index, and θ_k is a uniform random variable over $[0, 2\Pi)$.

According to the reports on channel measurements, the different channel environments are subject to the different Doppler spectrumand furthermore, the maximum Doppler frequency as well as Doppler spectrum may vary for each path. Figures 3.4(a) and (b) show two different paths, with the maximum Doppler frequency of 100 Hz and 10 Hz, respectively, which are generated by the modified frequency-domain and time-domain FWGN models with the Classical Doppler spectrum, respectively.

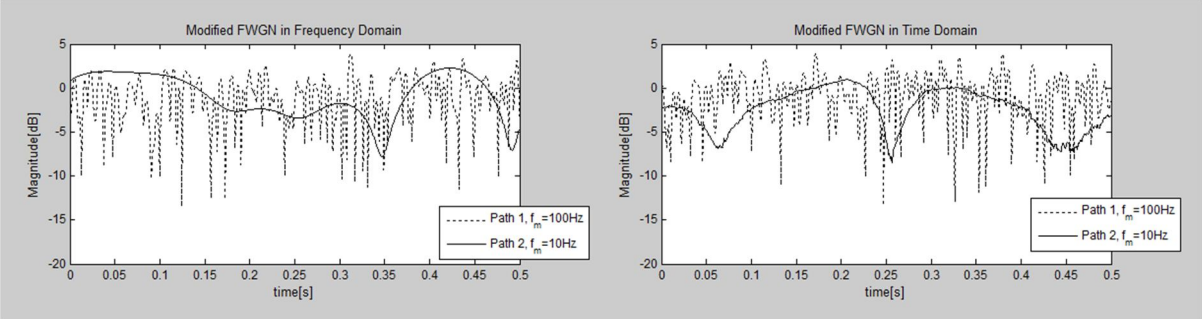

(a) Modified frequency-domain FWGN model (b) Modified time-domain FWGN model

Figure 3.4 Generation of two different paths with FWGN channel model.

3) Time-Domain FWGN Model: As shown in Figure 3.5, we can generate the fading channel by filtering the complex Gaussian random process with the time-domain filter whose frequency response corresponds to the Doppler spectrum. Due to the various advantages of the time-domain FWGN model, it is frequently employed in the commercial channel simulators.

Figure 3.5 Time-domain FWGN model: an overview.

As opposed to the frequency-domain FWGN model in which the duration of fading channel is determined by the IFFT size of N_{Fading} and the frequency-domain oversampling factor of N_{os}, it is determined by the length of the complex Gaussian random signal in the time-domain FWGN model. Since the simulation interval can be extended simply by increasing the number of complex Gaussian random samples subject to the Doppler filter, it is flexible for simulation [16].

The FWGN channel model allows for employing various other types of Doppler spectrum, including the flat Doppler spectrum and Laplacian Doppler spectrum. The flat Doppler spectrumhas the constant power spectral density function, i.e.,

$$S(f)\alpha 1, |f| \le f_m \qquad (3.2)$$

Meanwhile, the Laplacian Doppler spectrum is defined by the following power spectrum density function:

$$S(f)\alpha \frac{1}{\sqrt{1-(f/f_m)^2}} \left\{ \exp\left(-\frac{\sqrt{2}}{\sigma} \left| \cos^{-1}(f/f_m) - \phi \right| \right) + e \exp\left(-\frac{\sqrt{2}}{\sigma} \left| \cos^{-1}(f/f_m) + \phi \right| \right) \right\}, |f| \le f_m \qquad (3.3)$$

where s is the standard deviation of PAS, and f is the difference between direction of movement (DoM) and direction of arrival (DoA). Unlike the flat or classical Doppler spectrum model, the mobile direction can be accounted into the Laplacian Doppler spectrum.

ISSN: 2321-9653; IC Value: 45.98; SJ Impact Factor: 7.177
Volume 7 Issue V, May 2019- Available at www.ijraset.com

B. Jakes Model

ARayleigh fading channel subject to agivenDoppler spectrumcan begenerated bysynthesizing the complex sinusoids. The number of sinusoids to add must be large enough to approximate the Rayleigh amplitude [24]. Figure 3.6 illustrates how the Jakes model is implemented. It has been assumed that all rays of the scattered components arriving in the uniform directions are approximated by N plane waves. Define $N_0 = (N/2-1)/2$ where $N/2$ is limited to an odd number. Let un denote an angle of arrival for the nth plane wave, which is modeled $\theta_n = 2\pi n/N, \text{n} = 1,2,.....,\text{N}_0$. As shown in Figure 3.6, a sum of N_0 complex oscillator outputs with the frequencies of $w_n = w_d \cos\theta_n, n = 1,2,....., N_0$, each corresponding to different Doppler shifts, is added to the output of a complex oscillator with a frequency of $w_d = 2\pi f_m$.

The real and imaginary parts, $h_I(t)$ and $h_Q(t)$, in the total sum of the complex oscillators can be represented respectively as

$$h_I(t) = 2\sum_{n=1}^{N_0}(\cos\phi_n \cos w_n t) + \sqrt{2}\cos\phi_N \cos w_d t \qquad (3.3a)$$

and

$$h_Q(t) = 2\sum_{n=1}^{N_0}(\sin\phi_n \cos w_n t) + \sqrt{2}\sin\phi_N \cos w_d t \qquad (3.3b)$$

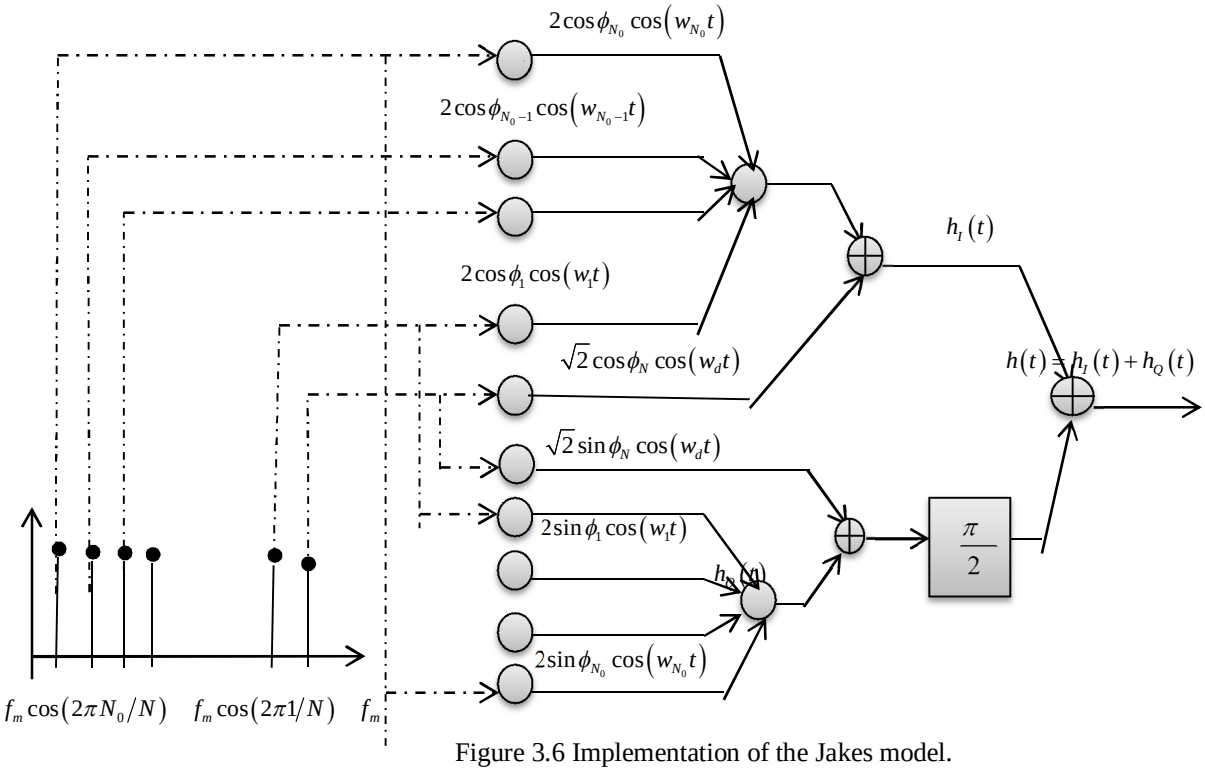

Figure 3.6 Implementation of the Jakes model.

where ϕ_n and ϕ_N are the initial phases of the n-th Doppler-shifted sinusoid and the maximum Doppler frequency f_m, respectively. The number of the Doppler-shifted sinusoids, N0, must be large enough to approximate the amplitude of the fading channel with a Rayleigh distribution. It has been known that $N_0 = 8$ is large enough. Note that the following properties can be shown for Equation (3.3):

$$E\left\{\left(\frac{E_0 h_I(t)}{\sqrt{2N_0+1}}\right)^2\right\} = E\left\{\left(\frac{E_0 h_Q(t)}{\sqrt{2N_0+1}}\right)^2\right\} = \frac{E_0^2}{2} \qquad (3.4)$$

$$E\{h^2(t)\} = E_0^2 \qquad (3.5)$$

$$E\{h(t)\} = E_0 \quad (3.6)$$

$$E\{h_1(t)h_Q(t)\} = 0 \quad (3.7)$$

Equation (3.5) and Equation (3.6) confirm that the Jake model generates the fading signal with the average amplitude of E_0 and average energy of E_0^2. Furthermore, Equation (3.4) and Equation (3.7) show that the real and imaginary parts of the channel are statistically independent with the average power of $E_0^2/2$.

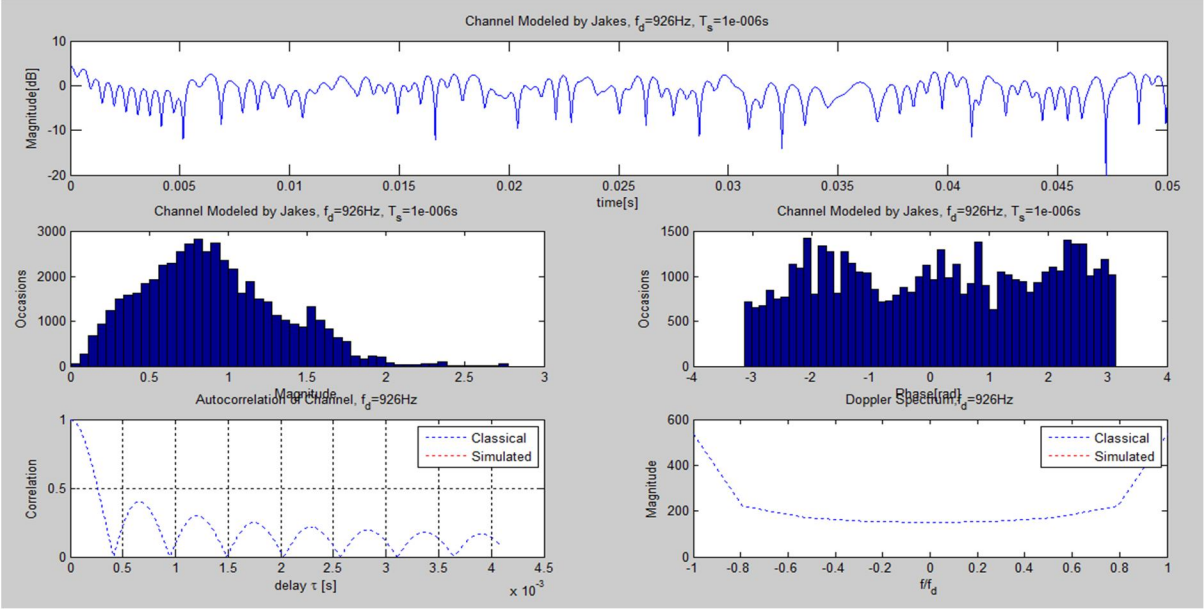

Figure 3.7 Generation of a time-varying channel with Jakes model. (a) Time-domain channel characteristics (b) Distribution of magnitude (c) Distribution of phase (d) Autocorrelation function (e) Doppler spectrum

C. Ray-Based Channel Model

A ray-based model is frequently used in modeling a MIMO channel, since it can take a spatiotemporal correlation into account [26]. However, it can be also used for a SISO channel. Its fundamental principle is described in this subsection while its extension to the MIMO channel . As in the Jake's model, the ray-based model is given by a sum of the arriving plane waves. As shown in Figure 3.8, it can model the plane waves incoming from an arbitrary direction around the mobile terminal, which can deal with the various scattering environments. In general, its power azimuth spectrum (PAS) is not uniform. Unlike the Jakes model, therefore, its Doppler spectrum is not given in the U-shape, but in various forms, depending on the scattering environments.

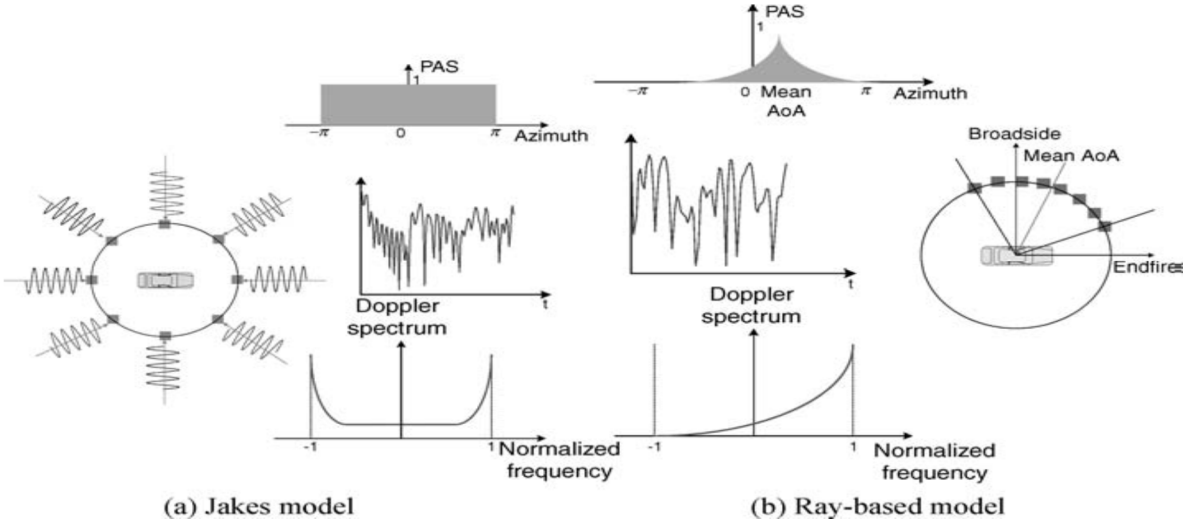

Figure 3.8 Difference between Jakes model and ray-based model.

ISSN: 2321-9653; IC Value: 45.98; SJ Impact Factor: 7.177
Volume 7 Issue V, May 2019- Available at www.ijraset.com

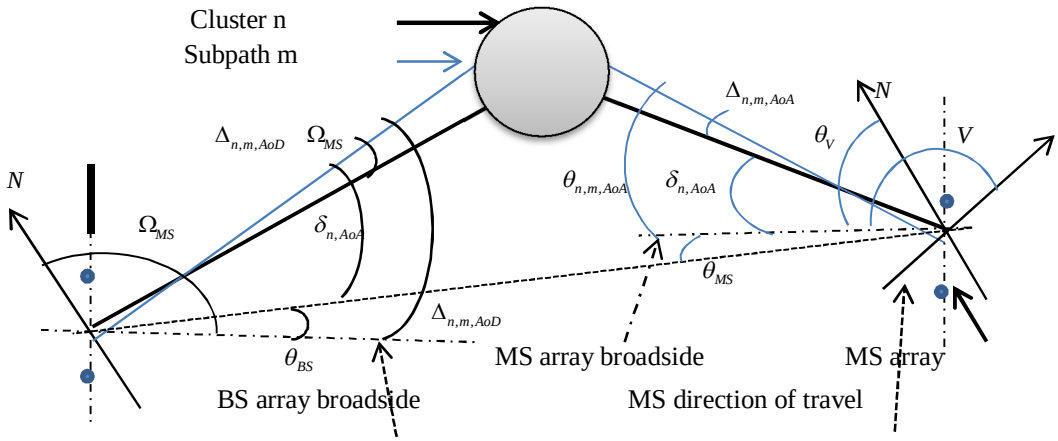

Figure 3.9 Ray-based MIMO channel model

Figure 3.9 shows one of the Ray-based channel models, known as a spatial channel model (SCM) for a MIMO channel in 3GPP [28]. Let $h_{u,s,n}(t)$ denote a channel impulse response of the nth path (cluster) between the sth transmit antenna and uth receive antenna, which can be represented as [28]

$$h_{u,s,n}(t)=\sqrt{\frac{P_n\sigma_{SF}}{M}}\sum_{m=1}^{M}\left(\begin{array}{l}\sqrt{G_{BS}(\theta_{n,m,AoD})}\exp\left(j\left[kd_s\sin(\theta_{n,m,\mathrm{AoD}})+\phi_{n,m}\right]\right)\\ \times\sqrt{G_{MS}(\theta_{n,m,AoA})}\exp\left(jkd_u\sin(\theta_{n,m,\mathrm{AoA}})\exp(\mathrm{jk}\|V\|\cos(\theta_{n,m,\mathrm{AoA}}-\theta_v)\mathrm{t})\right)\end{array}\right) \quad (3.8)$$

where

P_n : power of the nth path

σ_{SF} : standard deviation of log-normal shadowing

M: the number of subrays per path

$\theta_{n,m,\mathrm{AoD}}$: angle of departure of the mth subray for the nth path

$\theta_{n,m,\mathrm{AoA}}$: angle of arrival (AoA) of the mth subray for the nth path

$\phi_{n,m}$: random phase of the mth subray for the nth path

$G_{BS}(\theta_{n,m,AoD})$: BS antenna gain of each array element

$G_{MS}(\theta_{n,m,AoA})$: MS antenna gain of each array element

k : wave number $2\pi/\lambda$ where λ is the carrier wavelength

d_s : distance between antenna element s and reference antenna element (s=1) in BS

d_u : distance between antenna element u and reference antenna element (u=1)in MS

$\|V\|$: magnitude of MS velocity vector

θ_v : angle of MS velocity vector

ISSN: 2321-9653; IC Value: 45.98; SJ Impact Factor: 7.177
Volume 7 Issue V, May 2019- Available at www.ijraset.com

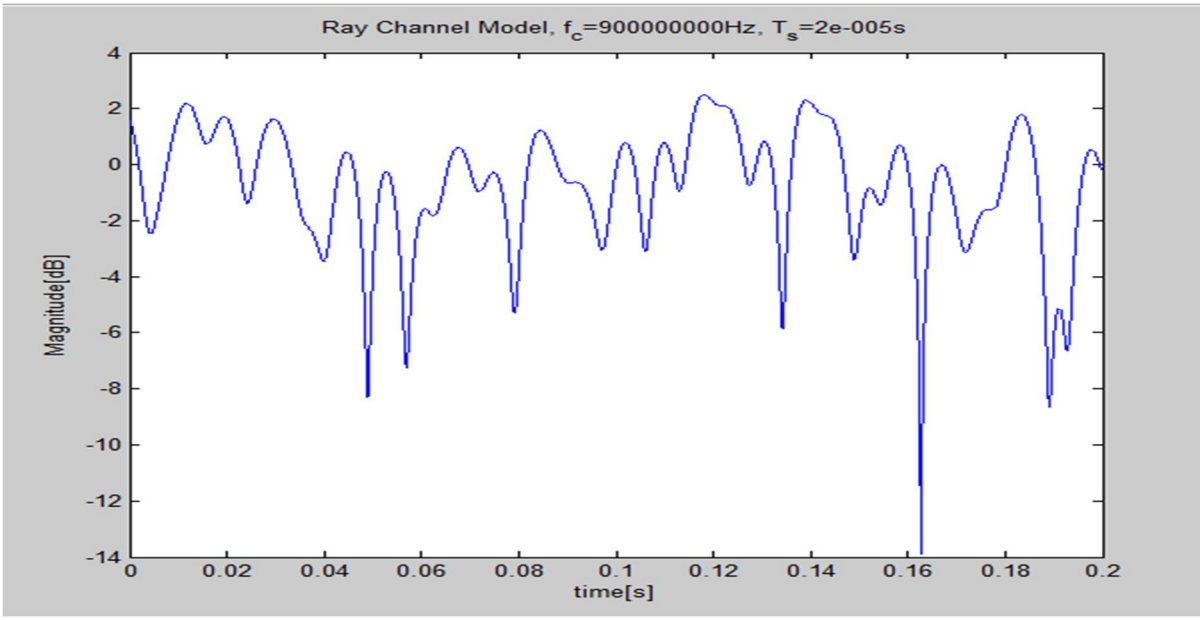

Figure 3.10 Ray-Based Channel with Uniform Power Subray Method

A uniform power subray-based channel model can be generated to get an angle spacing for equal power Laplacian PAS in SCM(spatial channel model), to assign the AoA/AoD offset tomean AoA/AoD, to generate DoAs at BS/MS and a randomphase at BS, and to combine the phases of M subrays to generate complex channel coefficients for each path, respectively

D. SUI Channel Model

According to the IEEE 802.16d channel model , a suburban path loss environment has been classified into three different terrain types, depending on the tree density and path-loss condition. The SUI (Stanford University Interim) channel model deals with the same environment as in the IEEE 802.16d channel model. Using the different combinations of the channel parameters, it identifies six different channel models that can describe the typical three terrain types in North America [9, 10] .The details of the channel parameters for the different SUI models are summarized. Note that the different K-factors and st are set for the different antenna types, for example, directional or omni antennas [9, 10].

Terrain type	**SUI channels**
A	SUI-5, SUI-6
B	SUI-3, SUI-4
C	SUI-1, SUI-2

Table 3.1 SUI channel models for the different terrain types.

In the SUI channel models, the Doppler power spectrum (PSD) is modeled as the following truncated form:

$$S(f)=\begin{Bmatrix}1-1.72\,f_0^{\,2}+0.785\,f_0^{\,4}, & f_0\le 1\\ 0, & f_0>1\end{Bmatrix} \qquad (3.9)$$

where $f_0 = f / f_m$.

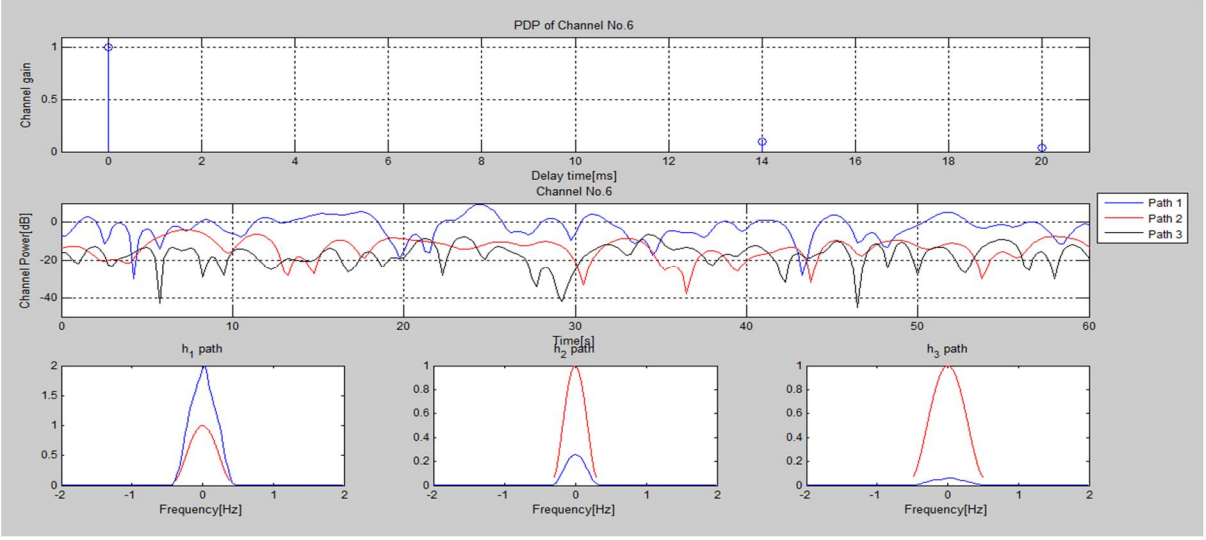

Figure 3.11 Channel characteristics for SUI-6 channel model. (a) Power delay profile (PDP) (b) Time-domain channel characteristic (c) PSD: *h*1 (d) PSD: *h*2 (e) PSD: *h*3

IV. CONCLUSION

In conclusion, it has been verified that the current channel model properly realizes the target channel characteristics. The contribution of this paper is an outdoor-to-indoor channel model fulfilling the requirements for simulations of mobile radio based positioning algorithms. The non-line-of-sight bias and the continuous evolution of multipath components with time are taken into account. A comparison of the channel model with the channel measurement data is performed by comparing statistics.

REFERENCES

[1] Sklar, B. (2002) Digital Communications: Fundamentals and Applications 2/E, Prentice Hall.
[2] Rappaport, T.S. (2001) Wireless Communications: Principles and Practice 2/E, Prentice Hall.
[3] Greenwood, D. and Hanzo, L. (1994) Characterization of mobile radio channels. Chapter 2, Mobile Radio Communications (ed. R. Steele), Pentech Press-IEEE Press, London.
[4] Friis, H.T. (1946) A note on a simple transmission formula. Proc. IRE, 34(5), 254–256.
[5] Lee, W.C.Y. (1985) Mobile Communications Engineering, McGraw Hill, New York.
[6] Okumura, Y., Ohmori, E., Kawano, T., and Fukuda, K. (1968) Field strength and its variability in VHF and UHF land mobile radio service. Rev. Elec. Commun. Lab., 16, 825–873.
[7] Hata, M. (1980) Empirical formula for propagation loss in land mobile radio services IEEE Trans. Veh. Technol., 29(3), 317–325
[8] Erceg, V., Greenstein, L.J., Tjandra, S.Y. et al. (1999) An empirically based path loss model for wireless channels in suburban environments. IEEE J. Select. Areas Commun., 17(7), 1205–1211.
[9] IEEE (2007) 802.16j-06/013r3. Multi-Hop Relay System Evaluation Methodology (Channel Model and Performance Metric).
[10] IEEE (2001) 802.16.3c-01/29r4. Channel Models for Fixed Wireless Applications.
[11] IST (2004) 4-027756. WINNER II, D1.1.1 WINNER II Interim Channel Models.
[12] Recommendation (1997) ITU-R M.1225. Guidelines for Evaluation of Radio Transmission Technologies for IMT-2000.
[13] Clarke, R.H. (1968) A statistical theory of mobile radio reception. Bell System Tech. J., 47, 987–1000.
[14] Capoglu, I.R., Li,Y., and Swami, A. (2005) Effect of doppler spread in OFDM based UWB systems. IEEE Trans. Wireless Commun., 4(5), 2559–2567.
[15] Stuber, G.L. (1996) Principles of Mobile Communication, Kluwer Academic Publishers.
[16] Tepedelenliglu, C. and Giannakis, G.B. (2001) On velocity estimation and correlation properties of narrow-band mobile communication channels. IEEE Trans. Veh. Technol., 50(4), 1039–1052.
[17] Andersen, J.B., Rappaport, T.S., and Yoshida, S. (1995) Propagation measurements and models for wireless communications channels. IEEE Commun. Mag., 33(1), 42–49.
[18] Bajwa, A.S. and Parsons, J.D. (1982) Small-area characterisation of UHF urban and suburban mobile radio propagation. Inst. Elec. Eng. Proc., 129(2), 102–109.
[19] Bello, P.A. (1963) Characterization of randomly time-variant linear channels. IEEE Trans. Commun., 11(4), 360–393.
[20] Black, D.M. and Reudink, D.O. (1972) Some characteristics of mobile radio propagation at 836 MHz in the Philadelphia area. IEEE Trans. Veh. Technol., 21(2), 45–51.
[21] Corazza, G.E. and Vatalaro, F. (1994) A statistical model for land mobile satellite channels and its application to nongeo stationary orbit systems systems. IEEE Trans. Veh. Technol., 43(3), 738–742.
[22] Akki, A.S. and Haber, F. (1986) A statistical model of mobile-to-mobile land communication channel. IEEE Trans. Veh. Technol., 35(1), 2–7.

[23] IEEE (1996) P802.11-97/96. Tentative Criteria for Comparison of Modulation Methods.
[24] Saleh, A.M. and Valenzuela, R.A. (1987) A statistical model for indoor multipath propagation. IEEE J. Select. Areas Commun., 5(2), 128–137.
[25] IEEE (2003) 802.15-02/490R-L. Channel Modeling sub-committee. Report finals.
[26] Smith, J.I. (1975)Acomputer generated multipath fading simulation for mobile radio. IEEE Trans. Veh. Technol., 24(3), 39–40.
[27] Jakes, W.C. (1974) Microwave Mobile Communications, John Wiley & Sons, Inc., New York.
[28] 3GPP (2007) TR 25.996, v7.0.0. 3rd Generation Partnership Project; Technical Specification Group Radio Access Network; Spatial Channel Model For Multiple Input Multiple Mutput Simulations (Release 7).
[29] SCM (2002) 065v2. SCM Model Correlations.
[30] SCM (2002) 033-R1. Spatial Channel Model Issues.
[31] COST 207 (1989) Digital land mobile radio communications, _ECSC-EEC-EAEC, Brussels-Luxembourg,1989.
[32] Fleury, B.H. and Leuthold, P.E. (1996) Radiowave propagation in mobile communications: An overview of European research. IEEE Commun. Mag., 34(2), 70–81.
[33] Greenstein, L.J. (1978) A multipath fading channel model for terrestrial digital radio systems. IEEE Trans. Commun., 26(8), 1247–1250.
[34] Loo, C. (1985) A statistical model for a land mobile satellite link. IEEE Trans. Veh. Technol., 34(3), 122–127.
[35] Lutz, E. and Plochinger, E. (1985) Generating Rice processes with given spectral properties. IEEE Trans. Veh. Technol., 34(4), 178–181.
[36] Schilling, D.L. et al. (1991) Broadband CDMA for personal communications systems. IEEE Commun. Mag., 29(11), 86–93.
[37] Seidel, S.Y. et al. (1991) Path loss, scattering and multipath delay statistics in four european cities for digital celluarl and microcellular radiotelephone. IEEE Trans. Veh. Technol., 40(4), 721–730.
[38] Pedersen, K.I., Mogensen, P.E., and Fleury, B.H. (2000) A stochastic model of the temporal and azimuthal dispersion seen at the base station in outdoor propagationenvironments. IEEE Trans. Veh. Technol., 49(2), 437–447.
[39] Schumacher, L., Pedersen, K.I., and Mogensen, P.E. (2002) From antenna spacings to theoretical capacitiesguidelines for simulating MIMO systems. PIMRC'02, vol. 2, pp. 587–592.
[40] I-METRA, D2 (Feb. 1999) IST-1999-11729, MIMO channel characterisation.

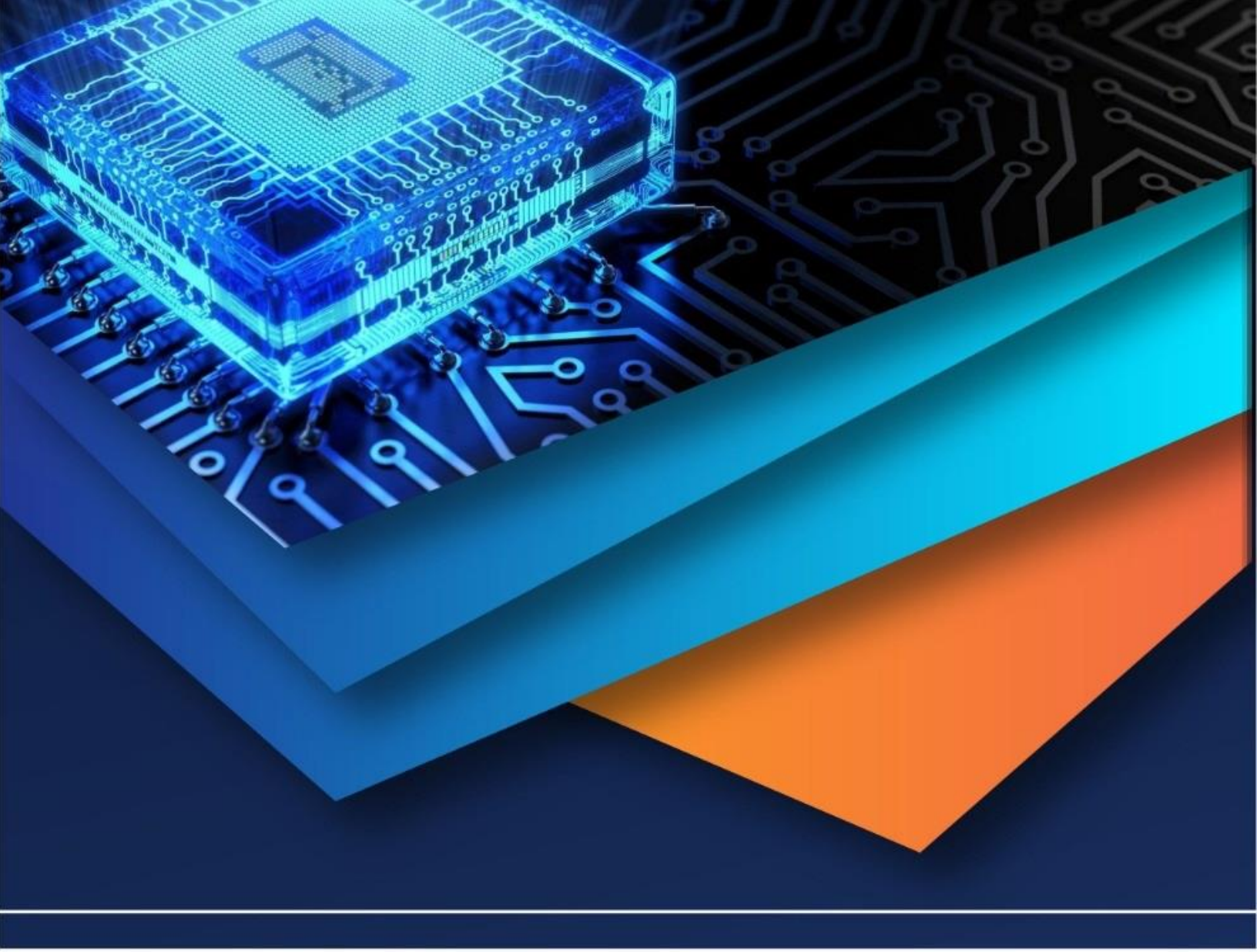

10.22214/IJRASET

45.98

IMPACT FACTOR: 7.129

IMPACT FACTOR: 7.429

INTERNATIONAL JOURNAL FOR RESEARCH

IN APPLIED SCIENCE & ENGINEERING TECHNOLOGY